Finexus: Tracking Precise Motions of Multiple Fingertips Using Magnetic Sensing

Ke-Yu Chen[1], Shwetak Patel[1], Sean Keller[2]

[1]University of Washington, DUB, UbiComp Lab
Seattle, WA, USA
{kychen, shwetak}@uw.edu

[2]Oculus Research
Redmond, WA, USA
sean.keller@oculus.com

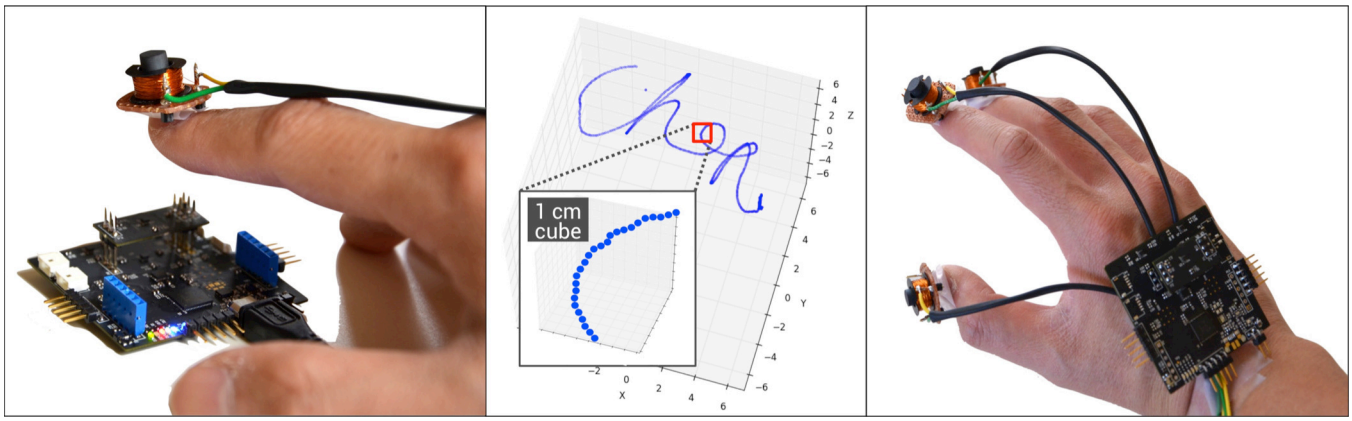

Figure 1: The *Finexus* system. (*Left*) Finexus can track the fine 3D motions of multiple electromagnets attached to fingertips using four magnetic sensors. (*Center*) The zoomed-in view shows the traces of precise finger movements within a 1 cm cube. (*Right*) The system leverages frequency multiplexing and a bandpass filter to achieve robustness against ambient noise.

ABSTRACT

With the resurgence of head-mounted displays for virtual reality, users need new input devices that can accurately track their hands and fingers in motion. We introduce *Finexus*, a multipoint tracking system using magnetic field sensing. By instrumenting the fingertips with electromagnets, the system can track fine fingertip movements in real time using only four magnetic sensors. To keep the system robust to noise, we operate each electromagnet at a different frequency and leverage bandpass filters to distinguish signals attributed to individual sensing points. We develop a novel algorithm to efficiently calculate the 3D positions of multiple electromagnets from corresponding field strengths. In our evaluation, we report an average accuracy of 1.33 mm, as compared to results from an optical tracker. Our real-time implementation shows Finexus is applicable to a wide variety of human input tasks, such as writing in the air.

CHI'16, May 07-12, 2016, San Jose, CA, USA
 ISBN 978-1-4503-3362-7/16/05…$15.00
DOI: http://dx.doi.org/10.1145/2858036.2858125

Author Keywords

Magnetic field; fingertips; tracking; 3D space; wearable; localization; electromagnet; real-time

ACM Classification Keywords

H.5.2 [Information interfaces and presentation]: User interfaces - Graphical user interfaces.

INTRODUCTION

Over the past few years, we have witnessed tremendous progress in wearable devices such as smart watches, fitness bands, and augmented reality (AR) / virtual reality (VR) devices. Existing user-input solutions for these devices rely on simple voice commands, a limited set of physical buttons, or gestures on a constrained touch areas (e.g., Google Glass's small touchpad). They are usually inconvenient, and can be socially awkward. Such input limitations can pose an even greater challenge when it comes to the use of head-mounted displays such as the Oculus Rift[1]. Ideally, interaction with a virtual world should involve not discrete gestures but rather the natural, continuous movements of the user's hands and fingers. Enabling this sort of natural interaction is also the key to giving people the sense that their virtual hands, which are rendered in virtual space, are actually their own hands. Accurately and efficiently tracking fine finger movements thus becomes important.

[1] Oculus Rift: https://www.oculus.com/en-us/rift

To achieve continuous hand tracking, researchers have explored computer vision (CV) techniques [18]. CV-based solutions, however, have occlusion issues, and the sensing area is limited to the view of the camera. An alternative approach leverages inertial measurement units (IMUs) for low-cost and occlusion-free gesture recognition [17]. Although effective, IMUs typically suffer from drift errors and may require frequent sensor calibrations. Strain gauge-based solutions (attached to a glove) are relatively effective, but the position of the strain gauge may shift on the glove when the hand changes pose; this may reduce tracking accuracy [20].

In order to address many of the shortcomings in existing hand-tracking solutions, we design *Finexus*, a 3D input device capable of tracking multiple fingertips using magnetic field (MF) sensing. The system continuously tracks fine finger movements, in real time, with electromagnets mounted on the backs of the fingers (see Figure 1 and the ***video*** figure). In order to enable multipoint tracking, we drive electromagnets using alternating current (AC) operating at distinct frequencies. By applying a bandpass filter centered at the corresponding frequency, the system is able to extract the magnetic fields generated from each individual electromagnet and remove unwanted noise (e.g., the Earth's magnetic field and ambient electrical noise). We design custom hardware and develop a novel algorithm to efficiently calculate the 3D position of multiple electromagnets from measurements of their magnetic fields. Because MF sensing is non-line-of-sight (NLOS), this system avoids the issue of occlusion inherent to optical-based tracking devices. Moreover, the MF sensing solution presented in this work does not suffer from drift, the fundamental limitation of IMUs.

We are not the first to apply MF sensing to object tracking. In the 1970s, Polhemus exploited MF sensing for tracking the motion of an object [23]. This system required large physical components in order to create three orthogonal magnetic fields, thus limiting system mobility. Instead of using electromagnets, some researchers have utilized magnetometers to track motions of a permanent magnet [1,7,14]. However, these systems only enable 1D, 2D, or limited 3D interaction, and are only able to track a single magnet. Finexus fuses these two approaches to enable accurate, multipoint tracking in 3D. Compared to Polhemus [23], we significantly shrink the electromagnet – to the size of a typical fingernail – and only utilize a 1D magnetic field for positioning. Using four magnetic sensors (only two more than in [7]), our novel algorithm is able to track multiple electromagnets in real time. This advancement allows flexible applications of this technique in different forms. For example, our sensor board could be embedded in a smartwatch or fitness band.

The core contributions of our work include:

1. A novel algorithm to efficiently track fine fingertip movements using only four magnetic sensors,
2. Custom hardware (*i.e.*, a PCB and electromagnets) to enable a continuous, multipoint tracking system in 3D,
3. Study and evaluation identifying precise tracking accuracies of 0.95 mm and 1.33 mm (fixed vs. random magnet orientation), and
4. The design and implementation of a real-time tracking system with a wide range of applications (e.g., typing on a keyboard, in-air writing, playing the piano, etc.).

RELATED WORK

Tracking hands and fingers has a long history in natural user interface (NUI) design [28]. In the 1980's, Kramer *et al.* leveraged a strain gauge attached to a glove to capture finger postures [20]. Although relatively effective, the position of the strain gauge on the glove shifts when the hand changes postures (e.g., when it transitions from an open hand to a closed fist). This typically causes significant loss of positional accuracy. IMUs have been used as an alternative approach [17]. Mycestro[2], for example, is an IMU-based commercial product for tracking finger movements. However, this device suffers from drift-based errors and may require frequent sensor recalibration.

Computer Vision-Based Approaches

With the exponential growth of computing power year after year, computer vision techniques have finally become a viable option for tracking accurate hand and finger motion. For example, Starner *et al*. designed an infrared (IR) camera, in pendant form, to capture and recognize various hand gestures [27]. Later researchers expanded this idea, and explored other on-body instrumentations. Kim *et al*. used an IR camera installed on the wrist to see the hand [18], Harrison *et al.* mounted a depth camera on the shoulder to detect finger touches on a user's arm [15], and Chan *et al.* leveraged a fisheye camera worn on the chest to detect whole-body gestures [3]. Several successful CV-based commercial products exist, such as Leap Motion[3], and other recent work leverages the built-in camera of a mobile phone to recognize various finger gestures [26]. Similarly, infrared proximity sensors have been used to obtain input in various ways [2]. While these methods may continuously track fine-grained finger postures, they can be sensitive to changing light conditions and suffer from occlusion issues, as they all require a line-of-sight view of the hands. Such limitations restrict the applicability of these techniques; one could not use these devices in a completely dark space or with a hand in a pocket.

On-Body Sensing

To mitigate occlusion issues, researchers have attempted non-CV-based sensing approaches. One technique uses electromyography (EMG) to sense tongue movements [31]. Deyle *et al.* discovered that different body movements can produce distinct sounds, which can be used as the basis for a gesture-based interaction system [9]. Making similar observations, Harrison *et al.* were able to identify finger

[2] Mycestro: http://www.mycestro.com
[3] Leap Motion: https://www.leapmotion.com

taps on an arm by analyzing the bio-acoustic sounds propagating through the human body [16]. Electric field (EF) sensing is another effective approach for detecting body and hand postures [8]. Some researchers have further applied EF sensing to convert compact fluorescent light (CFL) bulbs [10] or unmodified LCD monitors [6] into touch-sensitive surfaces. A limitation of these approaches is that they allow only interaction based on discrete gestures.

Indirect Sensing

Instead of on-body sensing, other researchers have instrumented the environment to enable hand and finger tracking. Pu *et al.* leveraged 2.4 GHz signals to enable whole-arm gesture recognition [22]. Doppler-shifted signals have also been shown to be a promising approach to detecting hand motions [5,11] or even nuanced chest movements (to estimate breathing rate) [24]. These techniques usually require accurate sensor calibration to obtain sufficient signal-to-noise ratios (SNR). They also rely on signal reflections from the human body and hence suffer from occlusion issues.

Magnetic Field Sensing

Magnetic field (MF) sensing is one clear approach for continuous, accurate, and occlusion-free finger tracking. Polhemus, by Raab *et al.*, is one of the earliest systems to leverage MF sensing, and can track objects with six degrees of freedom (DOF) [23]. Some commercial products, such as the Razer Hydra [4], use similar MF approaches in combination with IMUs to enable game-controller-based tracking. One major limitation of these works is that their base stations need to generate a strong 3-axis magnetic field, and thus must be relatively bulky. Furthermore, Polhemus leverages the gradient of the field (that is, the delta field obtained by subtracting two consecutive readings) to remove ambient noise. In order to avoid drifting issues with such an approach, the base station must be stationary, and to guarantee accuracy the three axes of fields must be time-synced. In addition, the user must stay within a narrow sensing range relative to the base station. These requirements make the system unsuited for portable use, especially for wearable applications. With Finexus, we address this problem by significantly shrinking the size of electromagnets and by utilizing 1D magnetic fields for positioning, and are thus able to make a wearable 3D-input device. More importantly, our new design allows both the sensors and electromagnets to freely move in space without any recalibration, and is thus applicable in dynamically changing scenarios (e.g., the sensors could be mounted in a smartwatch).

Instead of using a single magnetometer, some systems use arrays of magnetic sensors to track a magnetic element's 2D or 3D position. Yakukami *et al.* built a large driving coil and an array of pickup coils to track five LC-resonated markers worn on the fingertips [29, 30]. Liang *et al.* used an array of 192 Hall effect sensors to track the 2D positions of permanent magnets [21]. In related work, Chan *et al.* built a nail-sized 2D sensor array to convert the fingertip area into a mini touchpad with a permanent magnet worn on the thumb [4]. Unfortunately, these techniques require a relatively large sensor array, or enable only 2D positioning, and thus are limited as wearables.

Some researchers have leveraged off-the-shelf sensor boards or magnetometers built into a mobile device to track motions of a permanent magnet. Ashbrook *et al.* tracked the rotations of a magnetic ring to obtain 1D input to a smartwatch [1]. Attaching a permanent magnet to the nail, Harrison *et al.* enabled 2D input by tracking the radial positions of the magnet relative to a wearable device [14]. With a fixed and known sensor-magnet orientation, Han *et al.* showed that the 2D position of a permanent magnet can be calculated from a pair of magnetic sensors [12,13]. Chen *et al.* further extended Han's work to 3D positioning of a single permanent magnet [7]. Although low-cost and lightweight, these examples are only capable of 1D, 2D, or limited 3D interaction on a single magnet.

Among those MF sensing-based projects, our work is closest to, and motivated by, uTrack [7]. Despite their similarities, the two projects have fundamentally different goals, algorithms, and hardware/firmware requirements. uTrack was designed as a single-point tracking system and uses a strong permanent magnet to override ambient noise. Because the system does not remove surrounding noise (e.g., the Earth's magnetic field and electrical noise emitted from nearby electronic devices), the tracking accuracy significantly declines when the magnet moves just a few centimeters away from the sensors. In addition, the uTrack algorithm involves an exhaustive search of possible sensor orientations; this approach is computationally expensive and not practical for tracking multiple points. In contrast, Finexus targets a *multiple-point* tracking system. Our novel algorithm efficiently localizes multiple electromagnets without requiring a search of orientations. With the modest hardware requirement of only four magnetometers (compared to two magnetic sensors in [7]), our system is able to track multiple fingertips in real time. In our evaluation we find that our system, compared to the measurements of an optical tracker, has an average accuracy of 0.95 mm (with fixed magnet orientations) and 1.33 mm (with random orientations). We also implement a usable real-time system for Finexus, highlighting its capability to sense fine finger movements, e.g., writing in the air (see Figure 1 and the ***video*** figure).

THE FINEXUS SYSTEM

To localize electromagnets, Finexus leverages techniques similar to those used by the Global Positioning System (GPS). Intuitively, the system first calculates the distance between the electromagnet and four magnetic sensors, and then uses trilateration to identify the electromagnet's 3D position. Instead of solving three unknown orientations for

[4] Razer Hydra: http://sixense.com/razerhydra

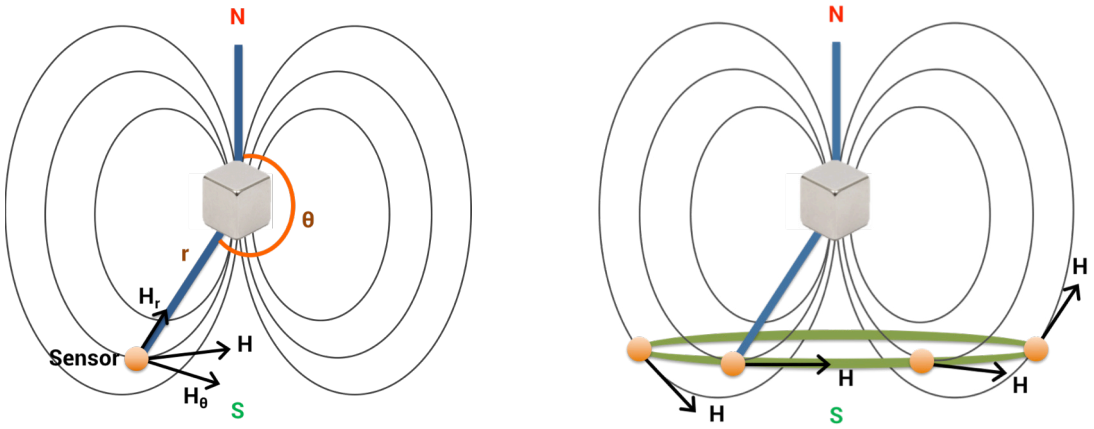

Figure 2: Magnetic field decomposition and spatial ambiguity. (*Left*) The magnetic field H can be decomposed into to two orthogonal vectors, $\mathbf{H_r}$ and $\mathbf{H_\theta}$. (*Right*) All points on a concentric circle (orange spots) have the same field strength. With unknown sensor orientations, these positions may have the same sensor reading, causing spatial ambiguity.

the 2D projection, we convert the magnetic field space into a beacon-like system and evolve an efficient algorithm for positioning multiple electromagnets. Below, we present requisite background information and discuss the challenges inherent to a magnetic field-based tracking system (Fig. 2). We then detail our methods for addressing these challenges to enable continuous multipoint 3D input; these include a predefined coordinate system (Fig. 3), a band-passed filter (Fig. 4), and custom hardware (Fig. 5 and Fig. 6).

Magnetism Primer

For an arbitrary location in space, the strength of magnetic field **H** can be defined with two factors, r (the distance between the magnet and the sensing point) and θ (the angle between the magnet's north and the sensing point). We usually decompose **H** into its components $\mathbf{H_r}$ (in the direction of the magnet) and $\mathbf{H_\theta}$ (orthogonal to $\mathbf{H_r}$). These two vectors are a basis for this 2D magnetic field space and can be mathematically represented in terms of r and θ (as shown in Fig. 2, left):

$$||\mathbf{H_r}|| = M \cos\theta / 2\pi r^3 \quad (1)$$

$$||\mathbf{H_\theta}|| = M \sin\theta / 4\pi r^3 \quad (2)$$

where M is the magnetic moment [19]. In the case of an electromagnet, the value of M relates to the permeability of core material, current flowing through the coils, and the cutaway section area of the electromagnet. Given an AC current with static peak-to-peak magnitude and a fixed size of the electromagnet, we can approximate M as a constant. We should note that this decomposition of H is only valid in certain conditions, specifically, when the excitation source is a coil and the distance from the coil is more than 4 times the radius of the coil. As we will detail in a later section, our algorithm leverages the total field strength and thus is not dependent on the decomposition, so this issue is avoided.

Unknown Orientation

To apply trilateration, the first step is to calculate the distance between the electromagnet and sensors. By solving Equations 1 and 2, we can readily calculate the distance (r) and orientation (θ) from the magnetic field ($\mathbf{H_r}$ and $\mathbf{H_\theta}$). However, there is ambiguity in 3D space. For example (as illustrated in Fig. 2, right), if we look at the electromagnet from the top, then points on a concentric circle have the same field strength, as they are all located at the same distance and angle from the electromagnet. With unknown sensor orientations, a sensor can report the same sensor measurement on these concentric positions – in other words, without knowing the orientation of the sensor, the decomposition of **H** in to $\mathbf{H_r}$ and $\mathbf{H_\theta}$ is ambiguous.

The traditional approach used to resolve this ambiguity is to apply a rotation matrix to transform the 3D sensor space to the 2D magnetic field space. After rotation, the sensor's x-axis and y-axis align with the directions of $\mathbf{H_r}$ and $\mathbf{H_\theta}$, respectively, and the hence the value of the third coordinate becomes zero. This transformation involves three unknown rotation angles and can be mathematically represented as:

$$\boldsymbol{T_{R,P,Y}}\,\mathbf{H} = \boldsymbol{T_{R,P,Y}} \begin{bmatrix} H_x \\ H_y \\ H_z \end{bmatrix} = \begin{bmatrix} \mathbf{H_r} \\ \mathbf{H_\theta} \\ 0 \end{bmatrix} = \begin{bmatrix} M \cos\theta / 2\pi r^3 \\ M \sin\theta / 4\pi r^3 \\ 0 \end{bmatrix} \quad (3)$$

where $\mathbf{H} = [H_x, H_y, H_z]^T$ is the sensor vector and $\boldsymbol{T_{R,P,Y}}$ is the rotation matrix with three unknown variables R (Roll), P (Pitch), and Y (Yaw).

Equation 3 reveals an under-constrained system; that is, we need to solve five unknown variables (R, P, Y, r, θ) using three equations (H_x, H_y, H_z). Solving these unknown angles (*i.e.*, R, P, Y) requires an exhaustive searching process to find the global optimal solution. Earlier work (from [7]) sub-optimized this search process by tracking the delta angle and reducing the complexity from three angles to two.

Although this is a significant reduction in the search space, this approach is still computationally expensive and not practical for tracking multiple points.

Resolving the Spatial Ambiguity

We evolve a completely different and efficient technique to calculate the distance r from the magnetic field. Specifically, we directly calculate the total magnetic field strength by merging three equations into one. The outcome is a new equation that can be written as:

$$\begin{aligned} ||\mathbf{H}||^2 &= (H_r)^2 + (H_\theta)^2 \\ &= K * r^{-6} * (3\cos^2\theta + 1) \end{aligned} \quad (4)$$

where $||\mathbf{H}||$ is the L-2 norm of the sensor vector, r and θ are the distance and tilt angle between the sensor and the electromagnet (same as in Eq. 1 and Eq. 2), and K is a constant. As the norm of the sensor reading is independent of the sensor orientation, this leaves only two unknown variables, r and θ.

The physical meaning of this simplification is to convert the 3D space into a *beacon system*. With a beacon, the received signal strength (*i.e.*, $||\mathbf{H}||$, the total magnetic field strength) only relates to the distance from the signal source (*i.e.*, r) and the signal receiving angle (*i.e.*, θ). With this 1D projection, we can avoid searching unknown rotation angles and significantly reduce the system complexity.

Equation 4, however, is still under-constrained, as we need to solve for two variables (r, θ) from a single equation (*i.e.*, $||\mathbf{H}||$). To obtain instead an over-constrained system, we leverage multiple sensors in a fixed, known layout. This layout defines a coordinate system; we will replace our two variables (r, θ) with the electromagnet's 3D position (x, y, z) in these new coordinates. Figure 3 shows the sensor topology and the coordinate system. In the current prototype, we choose sensor 1 (S1) as the origin. For each sensor, we have a pair of variables (r, θ); let (r_i, θ_i) be the pair corresponding to sensor i. These can be represented in terms of the electromagnet's 3D position (x, y, z):

$$\boldsymbol{r_1} = [x^2 + y^2 + z^2]^{1/2} \quad (5)$$

$$\boldsymbol{\cos\theta_1} = z/r_1 \quad (6)$$

Using the known relative positions of sensors 2, 3, and 4, we similarly obtain:

$$\boldsymbol{r_2} = [(x+1)^2 + (y-1)^2 + z^2]^{1/2} \quad (7)$$

$$\boldsymbol{\cos\theta_2} = z/r_2 \quad (8)$$

$$\boldsymbol{r_3} = [(x-1)^2 + (y-1)^2 + z^2]^{1/2} \quad (9)$$

$$\boldsymbol{\cos\theta_3} = z/r_3 \quad (10)$$

$$\boldsymbol{r_4} = [x^2 + y^2 + (z-1)^2]^{1/2} \quad (11)$$

$$\boldsymbol{\cos\theta_4} = (z-1)/r_4 \quad (12)$$

For each sensor we use Eq. 4 and substitute variables by way of equations 7-12 in order to generate an over-constrained system of four equations in three unknowns, (x, y, z).

It is worth noting that K, in Eq. 4, is a factor of the aforementioned constant M (in particular, $K = M^2 / 16\pi^2$) and is relevant to the electromagnet design. In Section DISCUSSION, we discuss this constant, K, in detail.

Tracking Multiple Points

Unlike [7], Finexus is able to simultaneously track multiple fingertips. Instead of using a permanent magnet, we leverage AC-driven electromagnets operating at different frequencies. By applying bandpass filters centered at these frequencies, our system can extract and differentiate the magnetic field emanating from individual electromagnets. The bandpass filter is a 6th order finite impulse response (FIR) filter with the 3 dB cutoff at +2 and -2 Hz from the center frequency. The data rate from the PCB is 320 samples/second, so the usable bandwidth is half of this, 160 Hz. Within this bandwidth, we drive our five electromagnets at 70 Hz, 85 Hz, 100 Hz, 115 Hz, and 125 Hz. The frequency selection approach taken in this work uses the widest possible bands while avoiding 60 Hz noise (and harmonics) emitted from surrounding electronic devices or the nearby power line infrastructure. We do not, however, perform an exhaustive frequency sweep to identify the best frequency for location tracking; we leave this as future work. It should also be noted that in Europe our frequency selection would need adjustment, as European electronic appliances operate at 50 Hz (excessive noise may be present at the 100 Hz harmonic).

Figure 4 illustrates one example of the filtering process on the z-axis of sensor 4. The raw sensor data (Fig. 4, top-left) contain multiple sinusoids from five electromagnets and a DC bias at approximately 500 mG (milli-gauss). After bandpass filtering the signal at 70 Hz, the time-domain data contain only the sinusoid wave of the target frequency (Fig. 4, top-right). We should note that the DC bias results from the Earth's magnetic field and can dynamically change with different sensor orientations. The bandpass filter not only eliminates electrical noise from nearby electrical devices, but also removes this strong DC noise from our signal. Compared to previous work [1,7,14] that leveraged a strong permanent magnet to overwrite the noise, this filtering

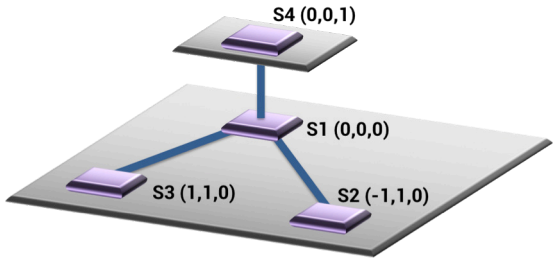

Figure 3: The coordinate system for trilateration. Using sensor 1 (S1) as the origin, we can easily infer the coordinates of the other three sensors (S2, S3, S4). S1, S2, and S3 are coplanar while S4 is directly above S1.

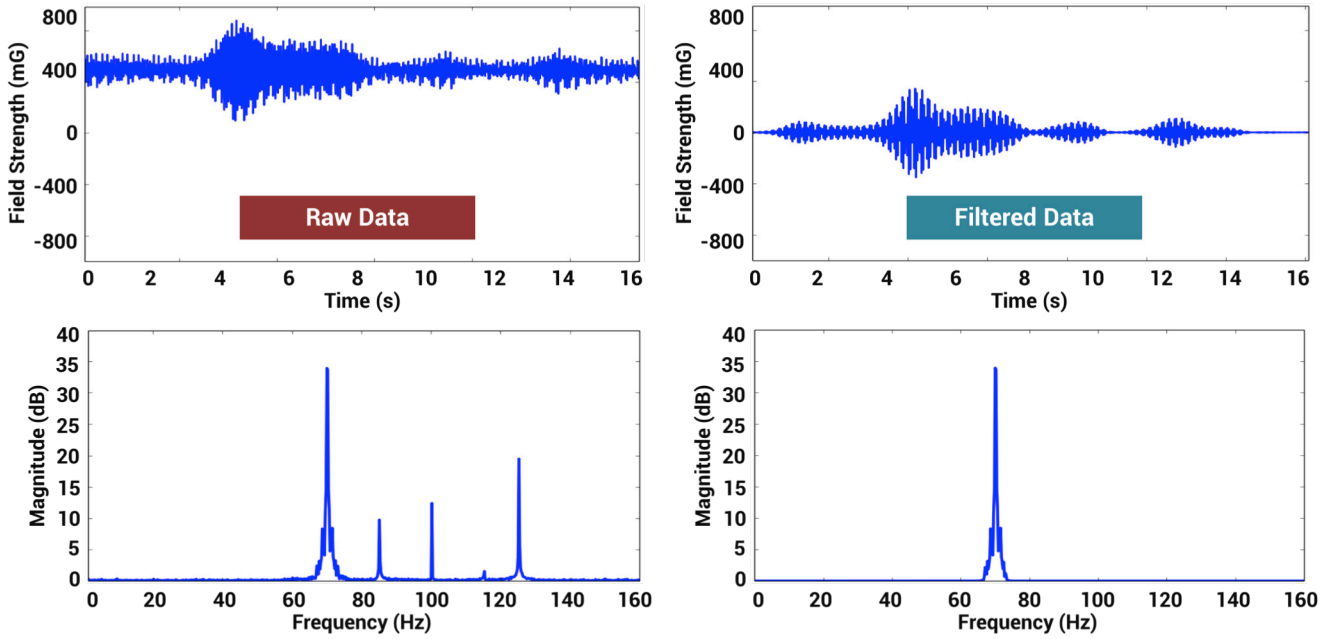

Figure 4: After band-passed filtering the raw time-domain data (*Top-Left*), the output is the magnetic field actuated by the specified electromagnet (*Top-Right*). The bottom two plots correspond to their frequency spectrums.

process cleverly removes it; this allows the system to operate with a weak magnetic field emitted from the electromagnet (~= 1/16 of the Earth's magnetic field). After we differentiate corresponding frequency components, we apply the Hilbert transform to extract the envelope of the sinusoid signal and feed the envelope curve (*i.e.*, the magnetic field strength) into our process pipeline.[5]

Algorithm and Process Pipeline

Our localization algorithm can be summarized in the following 5 steps:

1. Read the magnetic vector **H** from magnetic sensors and keep it in a sliding window of size 160
2. For each axis in **H**:
   - Apply the bandpass filter to extract magnetic fields emitted from individual electromagnets
   - Extract the envelope of the filtered data using the Hilbert transform
3. Calculate the L-2 norm of **H** (Eq. 4)
4. Substitute the variables r and θ in Equation 4 with x, y, z (Eq. 5 to Eq. 12)
5. Solve for the electromagnet's 3D position (x, y, z) and render the results

We should also note that the system always uses the current data point combined with the past 159 sensor vectors in Step 2 (*i.e.*, in total 160 data points in the sliding window). We choose a window size of 160 as double the bandpass filter window (*i.e.*, 80, in our design). For implementation, we adopt a 2-layer software architecture. In particular, we built our software using two languages to leverage strengths from both. The main process was a Java program that handles (1) data extraction from the PCB through the serial port, (2) multithreading worker threads, and (3) rendering the tracking results. Each worker thread (implemented in Python) runs the core signal processing for the individual electromagnets. The core algorithm (*i.e.*, steps 2 to 5) was implemented using the Numpy and Scipy libraries in Python.

HARDWARE

To support a high sampling rate for the frequency multiplexing and bandpass filtering process, we build a custom sensor board and electromagnets. In this section, we detail our hardware design.

PCB Design

Figure 5 (left) depicts the PCB and two sensor boards. The main board has a size of 5 cm x 5 cm and the daughter board, assembled on top of the main board, has a size of 1.3 cm x 2.6 cm. The purpose of the stacked-boards design is to create the coordination system for trilateration (Fig. 3). We determined optimal sensor placement following the guidelines of a previous study by Ray *et al.* where all sensors are equally spaced from the reference point [25]. In our design, we chose sensor 1 (S1) as the reference point (*i.e.*, the origin); sensors 2 and 3 (S2, S3) are co-planar with S1, while sensor 4 (S4) is directly above it. The latter three sensors (*i.e.*, S2, S3, S4) are 1 cm to 1.41 cm away from S1. In order to maintain maximum system flexibility, we place three PSoC microcontrollers (CY8C5266LTI-LP150) on both sides of the PCB to support up to 8 magnetometers. However the Finexus system only requires four magnetometers and one microcontroller, so the board could

[5] The Hilbert transform also serves as a lowpass filter and conveniently removes some sensor errors (if present).

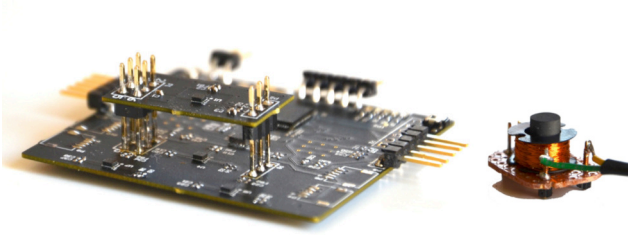

Figure 5: The PCB and electromagnet. (*Left*) The PCB has four magnetometers and three microcontrollers. (*Right*) The custom electromagnet has a cutaway section area of 0.25 cm^2 with 300 turns of coil.

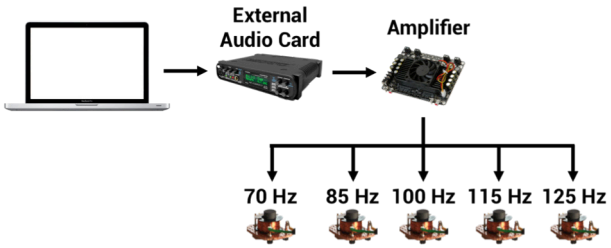

Figure 6: Five electromagnets are driven at corresponding frequencies from 70 Hz to 125 Hz. We sidestep 60 Hz and its harmonics to avoid possible electrical noise radiated from surrounding electronic devices.

be significantly reduced in size. In the current prototype, we sample the magnetometers (Memsic MMC3416xPJ) at 450 Hz with 14-bit resolution. Due to the overhead in synchronizing data in the 2-layer architecture (*i.e.*, one microcontroller at layer 1 and the other two at layer 2), the actual data rate drops to 320 Hz, which leaves a usable bandwidth of 160 Hz (*i.e.*, half of the Nyquist rate). This bandwidth is sufficient for driving five electromagnets (one for each fingertip).

Electromagnet

We handcrafted the electromagnets with a consistent design, as shown in Figure 5 (right). Each electromagnet was wrapped by 300 turns of coil and has a cutoff section area of 0.25 cm^2. We choose ferrite as the core material; it is an economical option and has a permeability of 32. To drive the electromagnets, we first synthesize sine waves using the media software MAX on a laptop. We next output the sinusoids to an external audio card (UltraLite mk3) that supports up to 10 channels, and then amplify the signal using a SURE Electronics TDA7498 amplifier board. Finally, the amplified signals are sent to individual electromagnets. Figure 6 depicts this process.

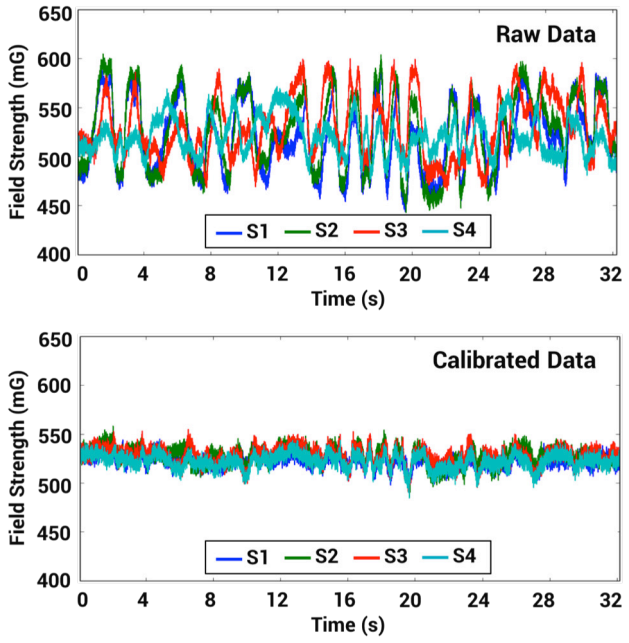

Figure 7: Magnetometer calibration. (*Top*) Raw data of the Earth's magnetic field include hard and soft errors. (*Bottom*) After calibration, four magnetic sensors (S1, S2, S3 and S4) present nearly uniform field strength.

It should be noted that at a distance of 60 mm, the magnetic field emitted from our electromagnets is roughly half the strength of the Earth's magnetic field. From Equations 1 and 2, the field strength significantly reduces – to 1/16 the Earth's field – when the distance is doubled (*i.e.*, 120 mm from the sensor). Even with such a relatively weak field, our system is still able to accurately track the fingertips. We discuss the tracking accuracy in section EVALUATION AND RESULTS.

Sensor Calibration

We follow standard procedure and use the Earth's magnetic field to calibrate the magnetometers. To collect data, we randomly rotate the PCB at a fixed location while keeping the PCB away from surrounding electronic devices to minimize noise. Figure 7 shows the calibration results. The raw data of different magnetometers are biased and scaled-shifted due to hard-/soft-iron effects (Fig. 7, top). After calibration, the sensor errors are removed; all magnetometers output nearly uniform field strengths (Fig. 7, bottom).

EVALUATION AND RESULTS

We evaluate the system by two metrics: (1) tracking accuracy and (2) computational cost. We obtain the ground truth data by using an NDI optical tracking system (Optotrack Certus [6]). This tracking system is configured to sample at 1 kHz and has a 3D accuracy of 0.1 mm. The optical markers are attached to both an electromagnet and the PCB (Fig. 9). As we use only a single camera, the optical marker on the electromagnet is occluded by the PCB or the user's hands in some orientations; the corresponding data points were discarded. The laptop for calculating the location and data collection was a MacBook Pro (mid 2014) with a quad-core 2.5 GHz processor and 16 GB RAM.

[6] NDI tracker: http://www.ndigital.com/msci/products/optotrak-certus

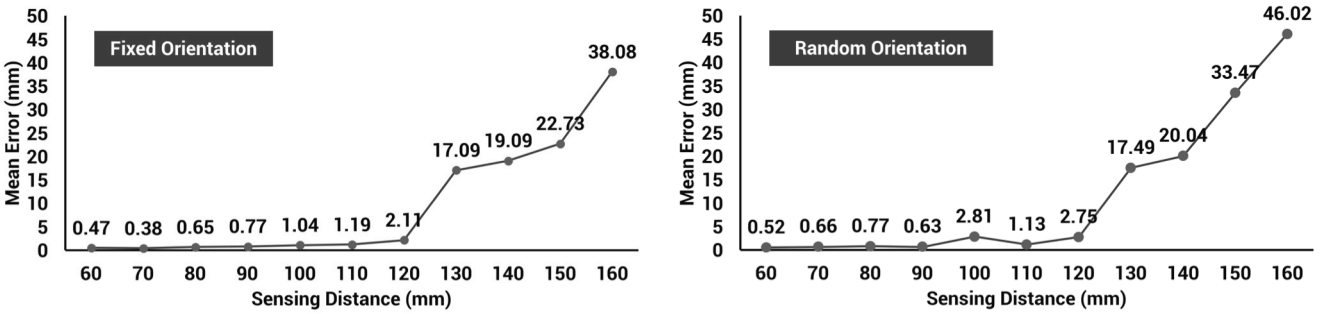

Figure 8: The tracking error vs. sensing distances under different magnet orientations. (*Left*) When the orientation of the electromagnet is fixed, we report an average error of 0.95 mm within 120 mm sensing distance. (*Right*) Allowing random orientations, our system still accurately tracks the electromagnet, with a similar tracking error of 1.33 mm.

Tracking Accuracy

Study Design

We first evaluated the tracking accuracy. To collect ground-truth data, we attached the PCB to the table and moved the electromagnets in a 3D volume (a 300 mm cube) centered at the sensor. We collected two datasets based on the magnet orientations: (1) in the first dataset, the electromagnet remained at a fixed orientation (that is, the electromagnet's north pole aligned with the sensor's x-axis), and (2) in the second dataset, we randomly rotated the electromagnet and moved it around in roughly the same volume. Separating these two datasets allows us to observe the influence of different magnet orientations and their impact on system robustness. To ensure temporal consistency, both the PCB and optical tracking system streamed data to the same computer and shared the same wall clock. In total, we collected 93397 data points for the offline analysis.

Results

Figure 8 shows the results of tracking accuracy under different magnet orientations. The mean error is defined as the Euclidean distance between our tracking results and the positions reported by optical markers (*i.e.*, the ground truth). In the case of fixed magnet orientations (Fig. 8, left), we report an average error of 0.95 mm (σ=0.92) within the sensing distance of 120 mm. In our algorithm, we apply a bandpass filter to remove the Earth's magnetic field and electrical noise from surrounding interference. The residual outcome from this filtering process is the magnetic field actuated only by a specified electromagnet. As expected, the filter is able to yield a high-SNR signal and therefore a high tracking accuracy. In the case of random magnet orientations (Fig. 8, right), we observe similar results and report an average error of 1.33 mm (σ=1.23) within the same sensing distance of 120 mm.[7] This high tracking accuracy allows Finexus to track fine fingertip motions, which may be used for a variety of applications, such as gaming control or writing in the air.

In both cases (*i.e.*, fixed and random orientations), we notice that the tracking error significantly increases when the electromagnet is located at a distance of 130 mm or more from the sensors. As we mentioned earlier, the magnetic field actuated from electromagnets drops to only 1/16 of the Earth's field (*i.e.*, ~= 0.03 G) at a distance of 120 mm. Given our sensor sensitivity (*i.e.*, 14 bits over 16 gauss), this is the lower bound of the required field strength to accurately track our electromagnet. This sensing distance could be extended by redesigning the electromagnets or using a better sensor (see section DISCUSSION for elaboration).

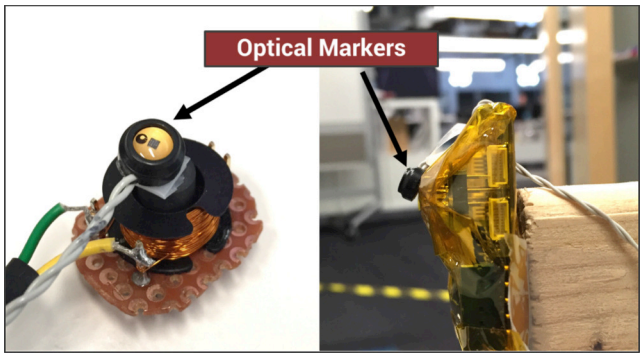

Figure 9: Collecting ground truth data. The optical trackers are attached to both the electromagnet (*left*) and the sensor board (*right*).

Computational Cost

Study Design

In the second analysis, we use the same datasets to evaluate the computational cost of our algorithm. The computational cost is defined as the total time to process a data point in the pipeline, that is, the amount of time from when a data point enters the process pipeline until the result is ready to render. As we target a real-time system, the purpose of this analysis is to identify required computational time and possible delay.

[7] We should note that there may be inaccuracy in the optical tracking system, which may impact the evaluation results.

Results

Using the same datasets, we report an average computational time of 2.22 ms per data point. This computational time is smaller than the sampling period (3.13 ms, as our data rate is 320 Hz), which confirms that our system is able to operate in real time. In the current prototype, we initiate separate worker threads for individual electromagnets. We can expect that the computational cost will linearly increase with the number of sensing points (e.g., tracking all 19 finger joints). In order to support higher tracking capacity, it is necessary to improve our implementation or to leverage extra hardware such as GPUs; we leave this as future work.

DISCUSSION

In this section, we discuss the limitations of the current prototype, propose possible improvements, and plan some future work.

Redesign the Electromagnet

In order to maintain sufficient field strength, we designed a relatively large electromagnet (Fig. 5, right). Although functional, the electromagnet is bulkier than ideal and may cause some usability concerns in real applications. In those instances, we would want to redesign the electromagnet and further shrink the size.

The design of the electromagnet is related to the constant $\boldsymbol{K}$ in Equation 4, which is proportional to four factors:

$$\boldsymbol{K} \propto \boldsymbol{\mu} * \boldsymbol{N} * \boldsymbol{I} * \boldsymbol{A} \quad (13)$$

where $\boldsymbol{\mu}$ is permeability, $\boldsymbol{N}$ is the turns of coil, $\boldsymbol{I}$ is the current flowing through the coil, and $\boldsymbol{A}$ is the cutaway section area of the electromagnet. The value of permeability indicates the ease with which magnetic fluxes flow through the core material. Using a core material with a larger permeability will generate a stronger magnetic field, if current, number of turns of coil, and magnet size are kept constant. In our current prototype, we choose ferrite as the core material. It is a practical option, but has a relatively low permeability (μ = 32). Using a different core material such as cobalt-iron, which has a much higher permeability (μ = 13000), we could drive the electromagnet with much smaller currents, reduce the size of electromagnets by a factor of 16 to 20, and simultaneously increase the magnetic field by a factor of four.

We should note that our system only requires a weak magnetic field for accurate tracking (*i.e.*, one that is roughly 1/16 field strength of the Earth's magnetic field) within a sensing distance of 120 mm. With the proposed electromagnet improvements, the sensing distance could potentially be extended to 15 cm; we leave the design, test, and validation as future work.

Enlarge Sensing Distance

Besides redesigning the electromagnet, another option for extending the sensing distance would be leveraging magnetometers with higher sensitivity. In our current prototype, we chose the Memsic mmc3416xPJ. This chip has three different configuration options: (1) 800 Hz sampling rate with a 12-bit resolution, (2) 450 Hz sampling rate with a 14-bit resolution, and (3) 250 Hz with a 16-bit resolution. In order to optimize the compromise between sampling frequency and resolution, we configured the magnetometer at 450 Hz with a resolution of 14 bits over 16 gauss (or 100 μT/count). We use a weak magnetic field for tracking, so this decrease in the sensor sensitivity (that is, from 16 bits to 14 bits) could cause a significant loss in sensing distance. Our goal is to use a new magnetometer at the same or higher sampling rate without trading away sensitivity. We have found a magnetometer manufactured by Yamaha (MS-3T) that has a sampling rate at 650 Hz and a much higher sensitivity – 1.2 μT/count. Combining this new magnetometer with redesigned electromagnets, we believe the sensing distance could be further extended, up to 25 cm.

Possible Applications

Although the current applications in virtual reality (VR) and augmented reality (AR) are still primarily computer games, we believe these burgeoning technologies will soon be applied to other domains (e.g., multimedia such as movies or music, education, or even clinical medicine). Given the precise tracking capability of our system, we envision a variety of applications that the Finexus system can enable within VR/AR. Besides in-air writing (see Fig. 1 and the ***video*** figure), possible applications range from basic gesture-based gaming control (e.g., first-person shooters and racing games) to complicated input that requires fine-grained actions (e.g., typing on a keyboard, painting, playing the piano, or using a TV remote in the virtual space). These applications are made possible by our system's robustness to ambient noise – by way of frequency multiplexing and bandpass filtering – that enables multipoint tracking without interference.

Possible Form Factors of Hand Instrumentation

One application of Finexus is as a hand-based input device. The electromagnets could be attached at the sensing points of interest (e.g., the fingertips or joints) and thin wires routed on top of the fingers. The sensor board could be incorporated into a smartwatch. With this vision in mind, we designed a 3D case for the sensor board and attached the electromagnets to the hand; Fig. 10 shows one possibility for such a hand instrumentation.

Combining With Other Sensors

Although we specifically designed Finexus for short-range, precise and multipoint tracking, the current prototype can be extended with additional sensors to enable more complex sensing capabilities. We have already assembled an IMU with 6 DOF on our sensor board. By instrumenting each electromagnet with one additional IMU (and by calculating its orientation relative to the sensor board), we could retrieve all 6 DOF of the electromagnets. Another possible extension of our current prototype is to build a

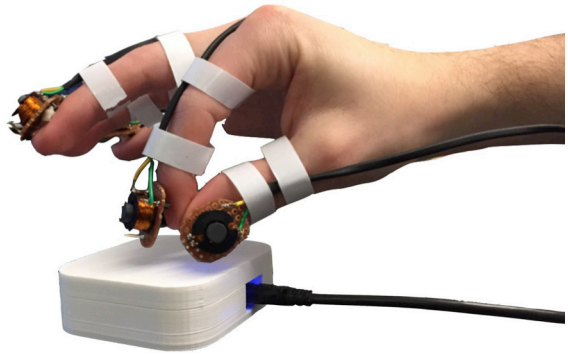

Figure 10: Possible hand instrumentation, including a 3D case for the sensor board (white box).

global coordinate system to yield the hand position relative to an AR/VR device in order to accurately render virtual hands. This can be achieved by embedding optical fiducials on a rigid body on the hand (or wrist). Another approach entails instrumenting an AC-driven coil on the AR/VR device to create a strong magnetic field at an alternate frequency to enable greater sensitivity at a distance. Further exploration is left as future work.

CONCLUSION

In this paper, we introduce a novel system that can track multiple fingertips in real time. We leverage weak magnetic fields emitted from electromagnets for localizing their 3D positions. By attaching electromagnets to the fingertips, our system is able to track fine fingertip motions. Instead of utilizing a 2D system that requires an exhaustive search of unknown angles, we convert the sensing space into a beacon-like system and use trilateration for positioning. To enable multipoint tracking, we drive individual electromagnets at distinct frequencies and apply a bandpass filter to extract the corresponding field strength. Our evaluation reports an average accuracy of 0.95 mm and 1.33 mm (at a fixed vs. random magnet orientation) within a sensing distance of 120 mm. As head-mounted displays become more commonplace and accessible to the public, the need for a multipoint and real-time finger-tracking system will become more important. We believe Finexus provides such a solution.

ACKNOWLEDGEMENTS

We thank Bruce Cleary, David Perek and Jonathan Browder for their assistance with the hardware design and for their helpful comments on this article.

REFERENCES

1. Daniel Ashbrook, Patrick Baudisch, and Sean White, Nenya: subtle and eyes-free mobile input with a magnetically-tracked finger ring, In Proc. of CHI'11, pp.2043–2046.
2. Alex Bulter, Shahram Izadi, and Steve Hodges, SideSight: Multi-“touch” Interaction Around Small Devices, In Proc. of UIST'08, pp.201–204.
3. Liwei Chan, Chi-Hao Hsieh, Yi-Ling Chen, Shuo Yang, Da-Yuan Huang, Rong-Hao Liang, and Bing-Yu Chen, Cyclops: Wearable and Single-Piece Full-Body Gesture Input Devices, In Proc. of CHI'15, pp.3001-3009
4. Liwei Chan, Rong-Hao Liang, Ming-Chang Tsai, Kai-Yin Cheng, Chao-Huai Su, Mike Y. Chen, Wen-Huang Cheng, and Bing-Yu Chen, FingerPad: private and subtle interaction using fingertips. In Proc. of UIST'13, pp.255–260.
5. Ke-Yu Chen, Daniel Ashbrook, Mayank Goel, Sung-Hyuck Lee, and Shwetak Patel, AirLink: sharing files between multiple devices using in-air gestures. In Proc. of UbiComp'14, pp.565–569.
6. Ke-Yu Chen, Gabe A Cohn, Sidhant Gupta, and Shwetak N Patel, uTouch: sensing touch gestures on unmodified LCDs, In Proc. of CHI'13, pp.2581-2584.
7. Ke-Yu Chen, Kent Lyons, Sean White, and Shwetak Patel, uTrack: 3D Input Using Two Magnetic Sensors, In Proc. of UIST'13, pp.237–244.
8. Gabe Cohn, Daniel Morris, Shwetak Patel, and Desney Tan, Humantenna: Using the Body as an Antenna for Real-Time Whole-Body Interaction. In Proc. of CHI'12, pp.1901–1910.
9. Travis Deyle, Szabolcs Palinko, Erika Shehan Poole, and Thad Starner, Hambone: A Bio-Acoustic Gesture Interface, In *Proc. of ISWC'07*, pp.3–10.
10. Sidhant Gupta, Ke-Yu Chen, Matthew S Reynolds, and Shwetak N Patel, LightWave: Using Compact Fluorescent Lights as Sensors, In *Proc. of UbiComp'11*, pp.65–74.
11. Sidhant Gupta, Daniel Morris, Shwetak Patel, and Desney Tan, SoundWave: Using the Doppler Effect to Sense Gestures, In *Proc. of CHI'12*, pp.1911-1914.
12. Xinying Han, Hiroaki Seki, Yoshitsugu Kamiya, and Masatoshi Hikizu, Wearable handwriting input device using magnetic field, In *Proc. of SICE'07*, pp.365–368.
13. Xinying Hana, Hiroaki Seki, Yoshitsugu Kamiya, and Masatoshi Hikizu. Wearable handwriting input device using magnetic field: 2nd report: Influence of misalignment of magnet and writing plane, *Precision Engineering* issue 34, pp.425–430.
14. Chris Harrison and Scott E Hudson, Abracadabra: wireless, high-precision, and unpowered finger input for very small mobile devices, In *Proc. of UIST'09*, pp.121–124.
15. Chris Harrison, Hrvoje Benko, and Andrew D Wilson, OmniTouch: wearable multitouch interaction everywhere, In *Proc. of UIST'11*, pp.441–450.
16. Chris Harrison, Desney Tan, and Dan Morris, Skinput: appropriating the body as an input surface, In *Proc. of CHI'10*, pp.453-462.

17. Edward Nelson Henderson, An Inertial Measurement System for Hand and Finger Tracking, *Master Thesis* 2015.
18. David Kim, Otmar Hilliges, Shahram Izadi, Alex Butler1, Jiawen Chen, Iason Oikonomidis, and Patrick Olivier, Digits: freehand 3D interactions anywhere using a wrist-worn gloveless sensor, In *Proc. of UIST'12*, pp.167–176.
19. Martin B Kraichman, Handbook of electromagnetic propagation in conducting media, 2nd Edition, Naval Material Command, 1976.
20. James Kramer, Peter Lindener, and William R George, Communication system for deaf, deaf-blind, or non-vocal individuals using instrumented glove, *US Patent US5047952*, 1988.
21. Rong-Hao Liang, Kai-Yin Cheng, Chao-Huai Su, Chien-Ting Weng, Bing-Yu Chen and De-Nian Yang, GaussSense: attachable stylus sensing using magnetic sensor grid, In *Proc. of UIST'12*, pp.319–326.
22. Qifan Pu, Sidhant Gupta, Shyamnath Gollakota, and Shwetak Patel, Whole-home gesture recognition using wireless signals, In *Proc. of MobiCom'13*, pp.27–38.
23. Frederick Raab, Ernest Blood, Terry Steiner, and Herbert Jones, Magnetic Position and Orientation Tracking System, *IEEE Transactions on Aerospace Electron System* 1979, pp.709–718.
24. Ruth Ravichandran, Elliot Saba, Ke-Yu Chen, Mayank Goel, Sidhant Gupta and Shwetak N Patel, WiBreathe: Estimating Respiration Rate Using Wireless Signals in Natural Settings in the Home, *IEEE PerCom'15*, pp.131–139.
25. Probir Kumar Ray and Ajay Mahajan, A genetic algorithm-based approach to calculate the optimal configuration of ultrasonic sensors in a 3D position estimation system, *Robotics and Autonomous Systems* 2002, Volume 41, Issue 4, pp.165–177.
26. Jie Song, Gabor Soros, Fabrizio Pece, Sean Ryan Fanello, Shahram Izadi, Cem Keskin, and Otmar Hilliges, In-air gestures around unmodified mobile devices, In *Proc. of* UIST'14, pp.319–329.
27. Thad Starner, Jake Auxier, Daniel Ashbrook, and Maribeth Gandy, The gesture pendant: a self-illuminating, wearable, infrared computer vision system for home automation control and medical monitoring, In *Proc. of* ISWC'00, pp.87–94.
28. David J Sturman and David Zeltzer, A survey of glove-based input, *IEEE Transactions on Computer Graphics and Applications* 1994, Volume 14, pp.30–39.
29. S Yabukami, S Hashi, T Ozawa, S. Hoshi, M. Toyoda, Y. Okazaki, and K.I. Arai, Development of a Position-Sensing System for a Wireless Magnetic Marker Using a Differential Pickup Coil, *Journal of the Magnetics Society of Japan* 2005, Volume 29, Issue 2, pp.146–152.
30. S Yabukami, K Ogasawara, H Saitoh, S. Hoshi, M. Toyoda, Y. Okazaki, and K.I. Arai, Development of a Fingertip Position-Sensing System using LC Resonated Markers, *Journal of the Magnetics Society of Japan* 2007, Volume 31, Issue 6, pp.439–444.
31. Qiao Zhang, Shyamnath Gollakota, Ben Taskar, and Raj P N Rao, Non-intrusive tongue machine interface, In *Proc. of CHI'14*, pp.2555–2558.